Polymer Testing 60 (2017) 253–259

Contents lists available at ScienceDirect

Polymer Testing

journal homepage: www.elsevier.com/locate/polytest

Material Properties

Synergistic effects on polyurethane/lead zirconate titanate/carbon black three-phase composites

Alex Otávio Sanches [a], Darcy Hiroe Fujii Kanda [a], Luiz Francisco Malmonge [a], Michael Jones da Silva [b], Walter Katsumi Sakamoto [a], José Antonio Malmonge [a, *]

[a] Universidade Estadual Paulista (UNESP), Faculdade de Engenharia, Câmpus de Ilha Solteira, Avenida Brasil, 56, Centro, 15385-000 Ilha Solteira, SP, Brazil
[b] Universidade Estadual Paulista (UNESP), Câmpus Experimental de Rosana, Avenida dos Barrageiros, 1.881, Centro, 19.274-000 Rosana, SP, Brazil

ARTICLE INFO

Article history:
Received 22 February 2017
Accepted 29 March 2017
Available online 6 April 2017

Keywords:
Polymer-matrix composite
Synergism
Anisotropy
Casting
Carbon black

ABSTRACT

Synergistic processes in hybrid composites have frequently been described in the literature over the past few years, opening doors to new studies and applications for this type of material. In this study, three-phase composites were obtained using polyurethane (PU) as the matrix, lead zirconate titanate (PZT) as the ferroelectric ceramic and carbon black (CB) as the conductive phase. The discussion is primarily focused on a comparison of the electrical, thermal and dielectric properties of three-phase composites with those of PU_CB and PU_PZT biphasic composites. The study describes a synergistic effect between the PU/PZT/CB phases involved in the generation of charges between the particles, implying better homogeneity of the composites as well as influence over the PU crystallization. The PU_CB conductivity profile showed a phenomenon of multi-step percolation thresholds attributed to the molecular structure and repulsive surface charge of CB particles. The surface charge phenomenon restricted the percolation curve analysis of the three-phase composites by means of classic percolation theory, shown by distortion of the critical exponents. The dielectric constant three-phase composites increased gradually as a function of CB in accordance with the percolation profile.

1. Introduction

Polymeric composites hold great interest for the scientific and industrial communities because their properties can be tailored to suit various applications [1]. Polymer/ferroelectric ceramic composites are garnering attention due to the exponential growth of the electronics industry. This drives the research for new materials with high permittivity, combining low dielectric loss, mechanical resistance and compatibility with printed circuits; these properties make these composites excellent candidates for embedded capacitors in passive circuits [2]. The most common type of polymer/ferroelectric ceramic composite found in the literature is biphasic, with a connectivity of 0–3. Many papers have investigated the influence of the matrix, the size, and the shape of ceramic grains, ceramic surface functionalization, etc. [3] on the electrical, optical and mechanical properties of the final product. However, with regard to dielectric properties, these materials are restricted to dielectric constant values of 50–70 at room temperature, which limits their use.

The manufacture of three-phase composites has been gaining attention due to the high dielectric constants obtained with the insertion of a third conductive phase, generally at a nanometric scale [4–7]. According to Tchmutin et al. [8], although some long-term studies of biphasic composites containing ferroelectric or conductive particles have been conducted, the study of composites containing both phases is still limited. This is due to the complexity of determining the influence of each phase on the final properties of these materials. The literature includes a range of studies that examine metallic particles, such as nickel (Ni), silver (Ag), copper (Cu), platinum (Pt) etc., as well as carbon nanotubes and graphene as the third phase [4–15]. The literature presents three-phase composites with a well-behaved profile based on the mixing rule and the percolation theory [4–15]. However, in many cases, their properties differ from those predicted, especially given the possible synergistic interactions related to the particle geometry of the hybrid fillers, filler interactions, filler concentrations and processing methods [16–29].

In this study, three-phase polyurethane/lead zirconate titanate/

* Corresponding author.
E-mail address: mal@dfq.feis.unesp.br (J.A. Malmonge).

http://dx.doi.org/10.1016/j.polymertesting.2017.03.031
0142-9418/

carbon black composites were fabricated and the morphological, thermal and electrical properties of the composites were investigated. We highlight the synergistic effect found between CB and PZT, which significantly improved the dispersions of PZT in the three-phase composites.

2. Material and methods

2.1. Materials

The polymer used as the matrix was nonionic aliphatic polyether-based polyurethane (PU), available from Chemtura Corporation (Rio Claro, Brazil) under commercial reference *PU W320*. Lead zirconate titanate (PZT) was purchased from APC International Ltd. (Mackeyville, USA) under reference *851*. Its characteristics include: relative dielectric constant (1 kHz) of 1950, Curie temperature of 360 °C, a density of 7.6 g/cm^3 and average particle size of 40 μm. The carbon black (CB) was supplied by Orion Engineered Carbons (Paulínia, Brazil) under commercial reference *Printex XE-2*. Its characteristics are: average particle size of 35 nm, a surface area of 1000 m^2/g, and a bulk density of 0.1 g/cm^3.

2.2. Composite preparation

2.2.1. PU_CB and PU_PZT biphasic composites

PU_CB and PU_PZT composites were manufactured taking into account the volume of the particulates in the composite in relation to the fixed mass of PU, according to Eq. (1). The filler was added to the polyurethane slowly and the mixture was stirred continuously for approximately 1 h. The dispersion was subjected to an ultrasonic bath for 30 min and subsequently stirred continuously for 1 h. It was then placed in the ultrasonic bath for a second time for 30 min and stirred for 30 min. Finally, the mixture was degassed under vacuum, stirred slowly for 1 h, poured onto glass slides (preheated to 60 °C), and spread using a film casting doctor blade. After 240 min in a conventional oven at 60 °C, the samples in film form were removed from the slides and pressed at 80 °C for a period of 1 min under a pressure of 9.81 × 10^5 Pa.

$$M_c = M_p.\ (\rho_c/\rho_p).(\varphi_c/1 - \varphi_c) \quad (1)$$

where M_p is the polymer weight, Mc is the filler weight, ρ_c and ρ_p are the densities of the filler and the polymer, respectively, and φ_c is the filler volumetric fraction.

2.2.2. PU_PZT_CB three-phase composites

Three-phase composites of PU_PZT_CB were fabricated, taking into account the volume of particulates in the composite in relation to the fixed mass of PU, according to Eq. (1). The composites were obtained by adding CB slowly to the polyurethane dispersion. The mixture was stirred for approximately 1 h, followed by an ultrasonic bath for 30 min. Subsequently, the PZT was added to the mixture. The mixture was then stirred for 1 h and subjected a second time to the ultrasonic bath for 30 min and stirred for 1 h. Finally, the mixture was degassed under vacuum, stirred slowly for 1 h and then the films were prepared in the same way as those obtained for biphasic composites. The composites were designated PU_PZT_CB(X/Y), where X and Y indicate the volume fraction of PZT and CB in the composite, respectively.

3. Characterization

The morphology of the cryogenically fractured surfaces of the composite films was analyzed using an EVO LS15—Zeiss scanning electron microscope. The samples were attached to aluminum stubs with conductive carbon tape and sputtered with gold prior to analysis. The images were collected in secondary and backscattering mode (BSD). The mean diameter of the PZT and CB agglomerates in the micrographs was calculated using ImageJ 1.45 software. About 200 structures were examined for each composition. The thermal behavior of the composites was characterized by a differential scanning calorimeter (DSC) from TA Instruments (New Castle, USA) model MDSC 2920. Samples between 10 and 15 mg were sealed in aluminum pans and subjected to a cycle of heating/cooling/heating at a temperature range of −30 to 250 °C, using a nitrogen atmosphere at a flow rate of 65 cm^3/min. The heating rate employed was 10 °C/min. The mean values for the melting temperature and enthalpies were obtained from the first heating. A second heating run did not add any extra information so it was not included in this work. For reference, the calculated values for the enthalpy of the composites were normalized with respect to the mass of the polymer present. From the enthalpy values, the relative crystallinity X_c of the composites was calculated as shown in Eq. (2) [30]:

$$X_c = \Delta H_m/\omega\ \Delta H_{100} \quad (2)$$

where ΔH_{100} is the melt enthalpy for pure PU, ω is the mass fraction of the polymer matrix in the composite, and ΔH_m is the sample melt enthalpy. For electrical and dielectric characterization, the samples were metallized with gold on both sides and kept in a chamber with humidity controlled to 22% of the relative humidity before the measurements were taken. Impedance spectroscopy was conducted using the Hewlett Packard 4192A impedance analyzer, coupled to a data acquisition system. The measurements were gathered in the frequency range of 10^3–10^6 Hz at room temperature. The voltage applied was 1V_{rms}. Electrical conductivity in the dc regime was obtained by the two-point method. Three samples were used to obtain the mean values, as well as the standard deviation for each composition.

4. Results

4.1. Scanning electron microscopy (SEM)

Fig. 1a presents the SEM images of the PU_PZT and PU_PZT_CB composites (25% vol CB). The surface of the biphasic composites exhibits greater roughness compared to the neat PU (inset in Fig. 1a), indicating an increase in energy dissipation during fracture owing to the presence of PZT. The micrographics obtained by BSE clearly showed the PZT agglomerations (white spots); most of these had a spherical shape, with a mean diameter of (40 ± 17) μm. The black spots observed in Fig. 1h are microvoids, which resulted from the high PZT concentration. The addition of CB substantially affected the PZT dispersion, as shown in Fig. 1m–q. In addition, the surface roughness decreased. For large amounts of PZT, such as 30–40%, some PZT agglomeration is still present (Fig. 1p, q). In the same way, CB agglomerates also occurred for high CB concentrations, as shown in BSD images by means of elliptical structures in dark contrast. These structures were analyzed by the contour of the elliptic silhouette in the fracture plane. Fig. 2 shows that a linear reduction of agglomerate size was observed as a function of PZT concentration and that these agglomerates tended to assume a spherical shape. The CB, when dispersed in liquids or polymeric solutions, can acquire surface charges, as postulated by Schueler [27]. Harbour et al. [28] demonstrated that such charges appear by a triboelectric process between CB particles and polymers. The charged particles cause mutual repulsion, thereby reducing or preventing the agglomeration from forming. At the same time, the shear in the system was intensified, with PZT helping the broken

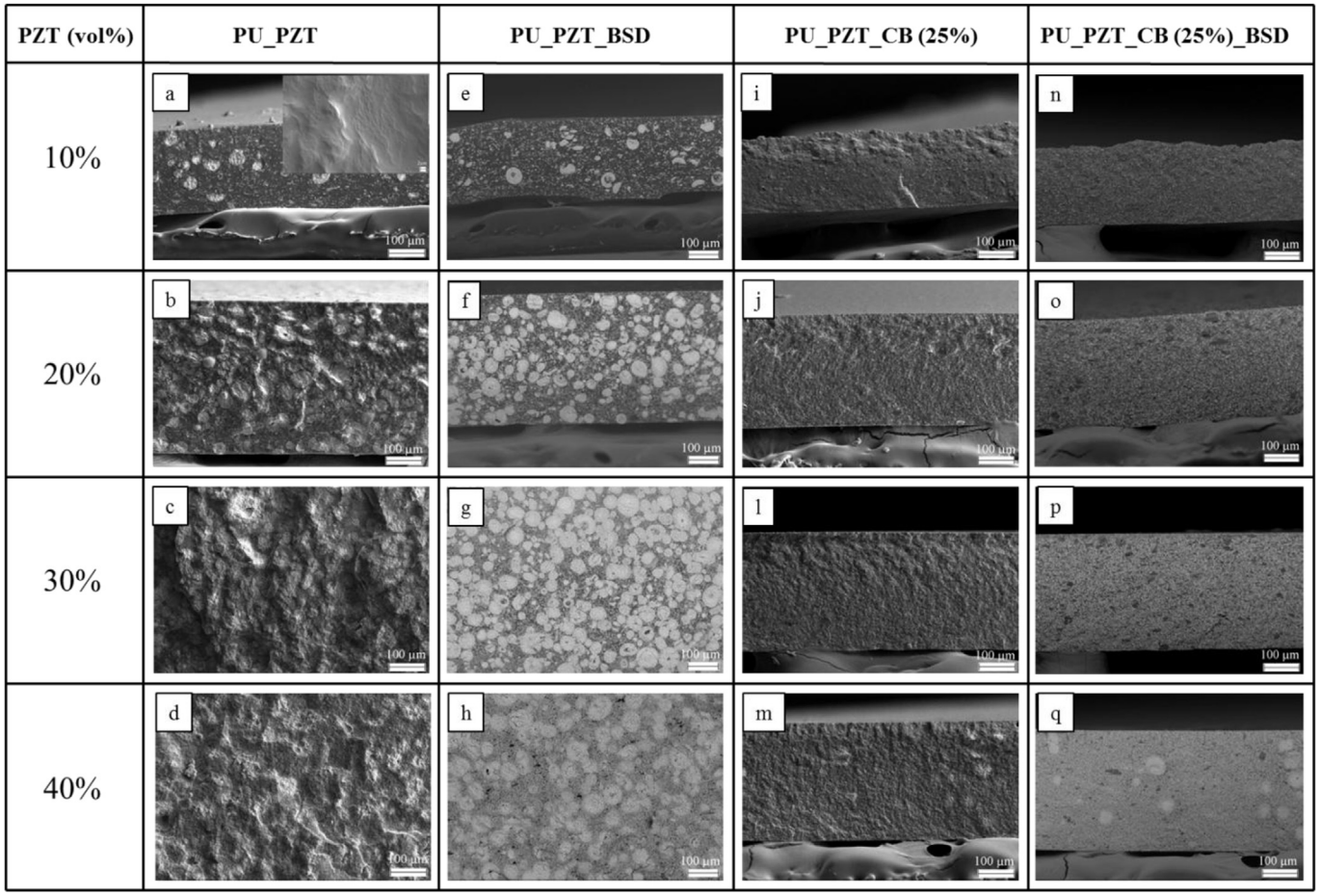

Fig. 1. SEM micrograph of PU_PZT and PU_PZT_CB for 25% CB vol. by secondary electrons and backscattered electrons. Inset shows PU micrograph by secondary electrons.

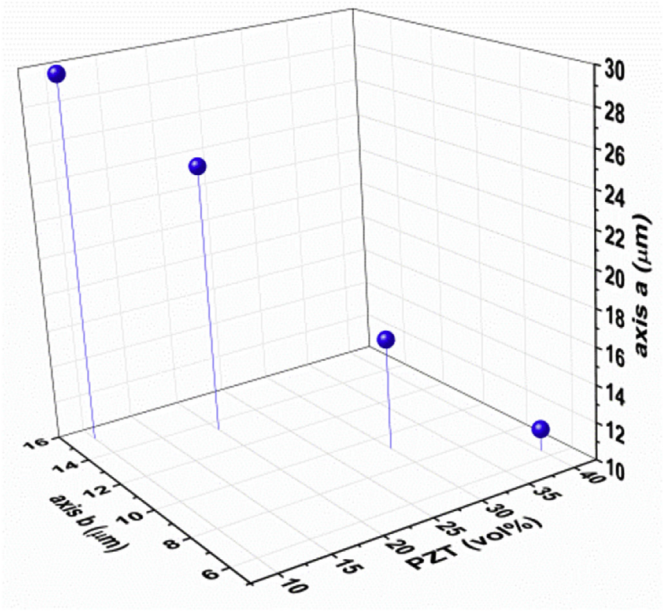

Fig. 2. Mean values of CB agglomerate size as a function of the PZT vol% for 25%vol CB.

agglomerates and strengthening the triboelectric effect. Some charged CB particles may adhere to PZT particles forming a PZT_CB system that repel each other, improving the PZT dispersion.

4.2. Electrical conductivity

The electrical conductivity of PU_CB as a function of CB content, and PU_PZT_CB as a function of PZT and CB contents, are depicted in Fig. 3a and b, respectively. As shown in Fig. 3a, the electrical conductivity increases gradually, rather than as a sharp, percolative insulator-conductor. This behavior has already been reported in the literature for PU_CB systems [31,32]. Segal [31] attributed this phenomenon to polyurethane's molecular structure, which is composed of alternating soft and hard segments, coupled with the high surface tension of PU. This tends to delay its ability to cluster, thus increasing the percolation threshold and generating a plateau in conductivity behavior. Hafiz [33] points out that the interface properties between the conductive phase and the polymer are responsible for the plateau observed in the polypirrole-PVC conductivity profile. However, as shown by Schueler [27], the Coulombic potential plays an important role in CB dispersion and agglomeration. In our case, the gradual, multi-step percolation curve of PU_CB shows that the Coulombic potential predominates over other factors and helps to improve dispersion; consequently, it contributes to elevating the percolation threshold to a high value (22% vol).

The insertion of PZT ceramics at the PU_CB binary phase significantly changes the electrical conductivity curve profile. A sharp percolation was observed for PU with 10% of PZT content, while no percolation threshold was found in the CB volume range studied for concentrations equal to or above 20% vol. For 10% vol PZT, the percolation threshold occurred at approximately 27% vol of

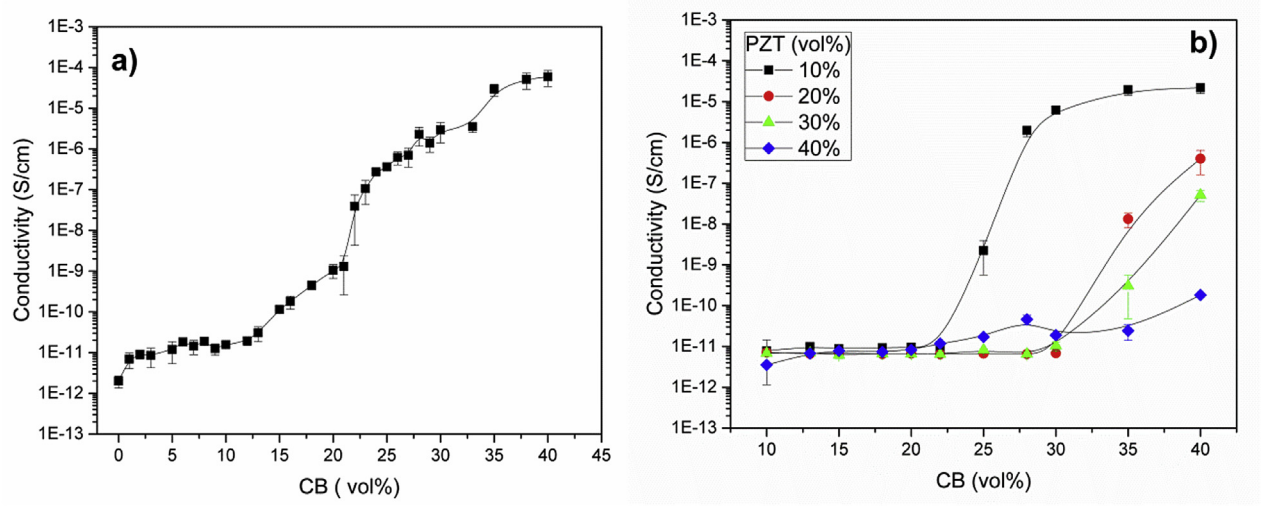

Fig. 3. Electrical conductivity of (a) PU_CB and (b) PU_PZT_CB composites.

the CB content. The addition of the third phase increased the effective concentration of CB in PU; accordingly, a decrease in the percolation threshold was expected, together with an increase in the PZT content [8]. However, the synergistic effect between PZT and CB helps their dispersion in the composite, delaying CB percolation. Increasing the PZT concentration also increases the insulating barrier, thus reducing the chances of a conductive path being formed.

According to percolation theory, the composites' conductivity near the percolation threshold is proportional to the power law (Eq. (3)):

$$\begin{aligned} \sigma &\propto (p - p_c)^t \quad p > p_c \\ \sigma &\propto (p_c - p)^{-s} \quad p < p_c \end{aligned} \tag{3}$$

where p_c is the percolation threshold, p is the CB fraction, and t and s are the critical exponents. In order to estimate p_c and the critical exponents for three-phase composites with 10% vol PZT composites, the conductivity data were plotted according to Eq. (3) by varying p_c in small intervals. For each value of p_c, values of t and s were obtained from the linear relationship between conductivity versus p-p_c and p_c-p on a log-log scale, respectively. The lowest value of the mean square error was found for $p_c = 28\%$, close to the threshold determined by the derivative of the log (σ) × CB vol% curve, which was 27%. The insets in Fig. 4 show the fitting obtained for threshold regions (p_c-p) and (p-p_c). It is verified that, for the region (p_c-p) below the percolation threshold, the points obtained from the plot show a marked dispersion, moving away from the power law (Eq. (3)), indicating that, in this region, the influence of the Coulombic potential is accentuated. As observed by McQueen [34], the dependence of conductivity on concentration in the region (p_c-p) is better described by an exponential function rather than a power law. In contrast, the region (p-p_c) presents better behavior and less dispersion due to the influence of the London-van der Waals potential. The critical exponents obtained were $s = 4.34$ and $t = 0.87$, differing from classic percolation theory. This fact is related to the highly non-random distribution of the conducting particles originating from the electrostatic repulsion in regions of the sample, given their heterogeneity and the simultaneous influence of the two potentials. The high value of the critical exponent s indicates the predominance of tunneling processes, and the conduction network forms a well-defined, percolation-like network. On the other hand, the low value of the critical exponent t suggests

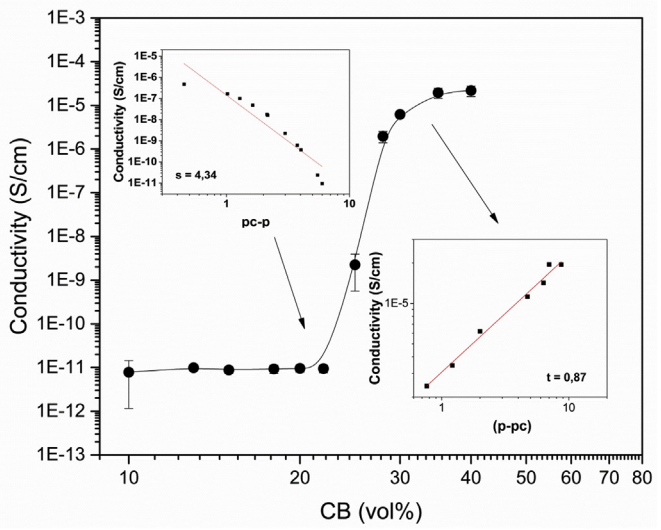

Fig. 4. Electrical conductivity of PU_PZT_CB with 10%PZTvol as a function of CB vol%.

that hopping and tunneling processes can also be included in the conduction mechanisms.

4.3. Thermal properties

Fig. 5a and b shows the DSC composites' thermograms for PU_PZT_CB, with 25 vol% CB and the melting temperatures for biphasic and three-phase composites, respectively. The parameters are summarized in Table 1. A single endothermic temperature peak around 44.9 °C was observed for neat PU (Fig. 5a) which was attributed to the melting of the crystalline phase (Tm) present in the soft domains [35]. For the composite PU_CB, the melting temperature shifted toward high temperature with increasing CB content, with a maximum at 5% vol (Fig. 5b). Furthermore, the enthalpy of fusion (ΔH) increases with increase of CB loading, compared to neat PU; this indicates that the relative crystallinity of PU (Xc) also increases. Carbon black acted as a nucleating agent in the soft phase, thereby increasing the crystallinity of the PU. However, for concentrations above 5% of CB in the binary composites, T_m, ΔH and X_c showed a downward trend occasioned by a

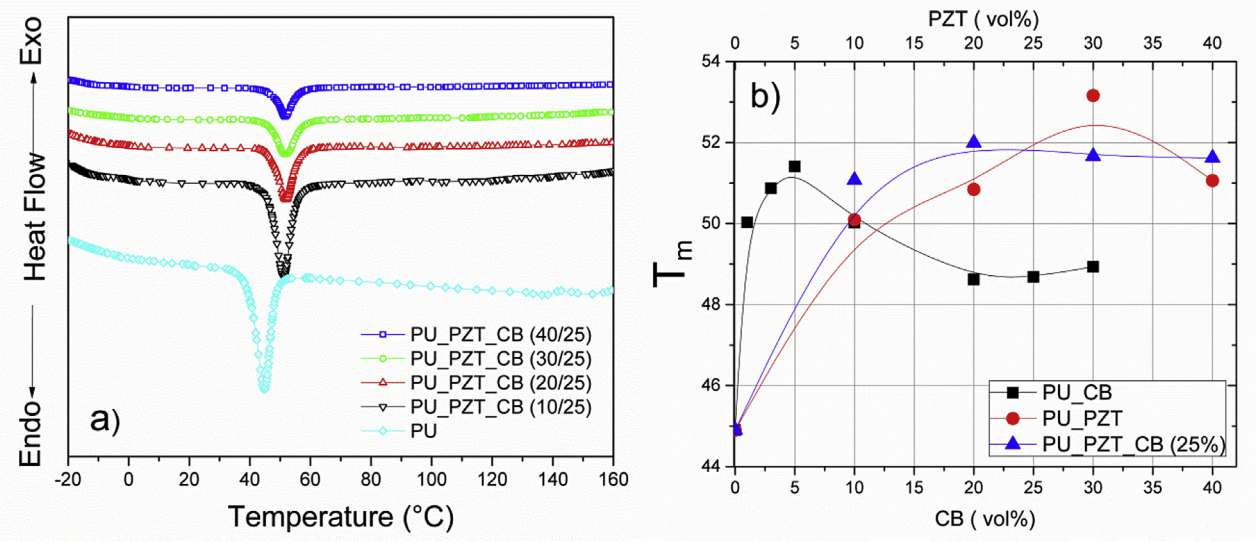

Fig. 5. (a) PU and PU_PZT_CB composites' thermograms; (b) Melting temperature of biphasic composites as a function of the vol% of CB or PZT and PU_PZT_CB for 25%vol CB as a function of the PZT vol%.

Table 1
Thermal parameters of PU_CB, PU_PZT and PU_PZT_CB composites.

Sample	T_m (°C)	ΔH (J/g)	X_c
PU	44,90	16,94	1,00
PU_1%CB	50,03	24,25	1,43
PU_3%CB	50,87	25,56	1,51
PU_5% CB	51,41	22,04	1,31
PU_10%CB	50,02	21,73	1,30
PU_20%CB	48,62	22,32	1,35
PU_25%CB	48,68	22,35	1,35
PU_30%CB	48,93	21,89	1,37
PU_10%PZT	50,09	12,15	1,20
PU_20%PZT	50,84	8,42	1,12
PU_30%PZT	53,16	6,50	1,11
PU_40%PZT	51,06	5,48	1,14
PU_PZT_CB(10/25)	51,07	29,30	1,73
PU_PZT_CB(20/25)	51,99	28,82	1,70
PU_PZT_CB(30/25)	51,66	30,12	1,77
PU_PZT_CB(40/25)	51,62	28,96	1,71

decrease in contact surface area of CB and PU due to the increased size of the carbon black agglomerates with CB concentration. For the PU_PZT composite, the T_m increased slightly, and gradually with increasing PZT content up to 30%. On the other hand, the enthalpy of fusion decreased; the crystallinity index remained higher than that of pure PU, but lower than that of PU_CB. These results indicate that the crystallites formed in the PU_PZT composites are smaller than those formed in both pure PU and PU_CB composites, as shown in Table 1. This occurs due to poor interaction between the matrix and the ceramic particles, as observed in the MEV micrograph. The PU_PZT_CB composites showed T_m higher than that of pure PU and the biphasic composites. This was attributed to the synergistic effect between the CB and PZT fillers, which was attributed to the improvement in the PZT and CB dispersion, as demonstrated by the MEV micrograph. The reduction of CB agglomerate size promoted a higher surface area of CB with PU contact causing a substantial increase in values, not only of T_m but also of ΔH and X_c of the three-phase composites compared to both PU and biphasic composites.

4.4. Impedance

Fig. 6a–d shows the dielectric spectra, obtained at room temperature, for composites with differing CB and PZT content. For binary PU_PZT composites, the dielectric constant increased with increasing the PZT content over the entire frequency range; however, the magnitude of the relative dielectric constant decreased slightly with increasing frequency, attributed to interfacial polarization [36,37]. When CB filler was present, the dielectric permittivity increased gradually as a function of the filler content to critical volume, which was dependent on PZT content; this correlated with the percolating curves and the repulsion charges hypothesis. The highest value of dielectric constant was found in the frequency range of 10^3–10^4 Hz between 25 and 35 wt% of CB. This behavior was attributed to interfacial polarization. The simultaneous influence of the fillers on ε and tg can be observed clearly in Fig. 7a and b, respectively, at a frequency of 1 MHz. The tendency of continuous increase of ε with the increase of the ferroelectric grains in the binary composites is contrasted with the insertion of the CB in concentrations of 30–40% vol, displacing the values of the peak for lower concentrations of PZT (the maximum is 30% vol PZT). The loss tangent (Fig. 7b) shows that, although the increasing insertion of the particles promotes an increase in the mechanisms of dielectrical loss, concentrations above 30% vol CB exert a reduction of tg due to the phase inversion process.

5. Conclusion

Three-phase composites employing PU as the matrix, PZT as the ferroelectric phase, and CB as the conductive phase were prepared in various compositions. The addition of CB to a PU_PZT binary composite substantially improved the PZT dispersion. A synergistic effect between the phases improved the CB surface charge; the CB may adhere to PZT particles, forming a PZT_CB system in which the particles repel one another, thus improving the PZT dispersion. The CB acts individually as a nucleating agent for the soft phase of the PU; this behavior was amplified by the synergistic effect between the phases. The electrical conductivity profile of PU_CB shows a multi-step percolation threshold attributed to the molecular structure of PU and the repulsive surface charge of CB particles. The "well-behaved" electrical conductivity curve was found in PU_PZT_CB, with 10 vol% PZT as a function of CB, compared to PU_CB. However, the analysis of the conductivity curve, based on classical percolation theory, showed a different value for universal

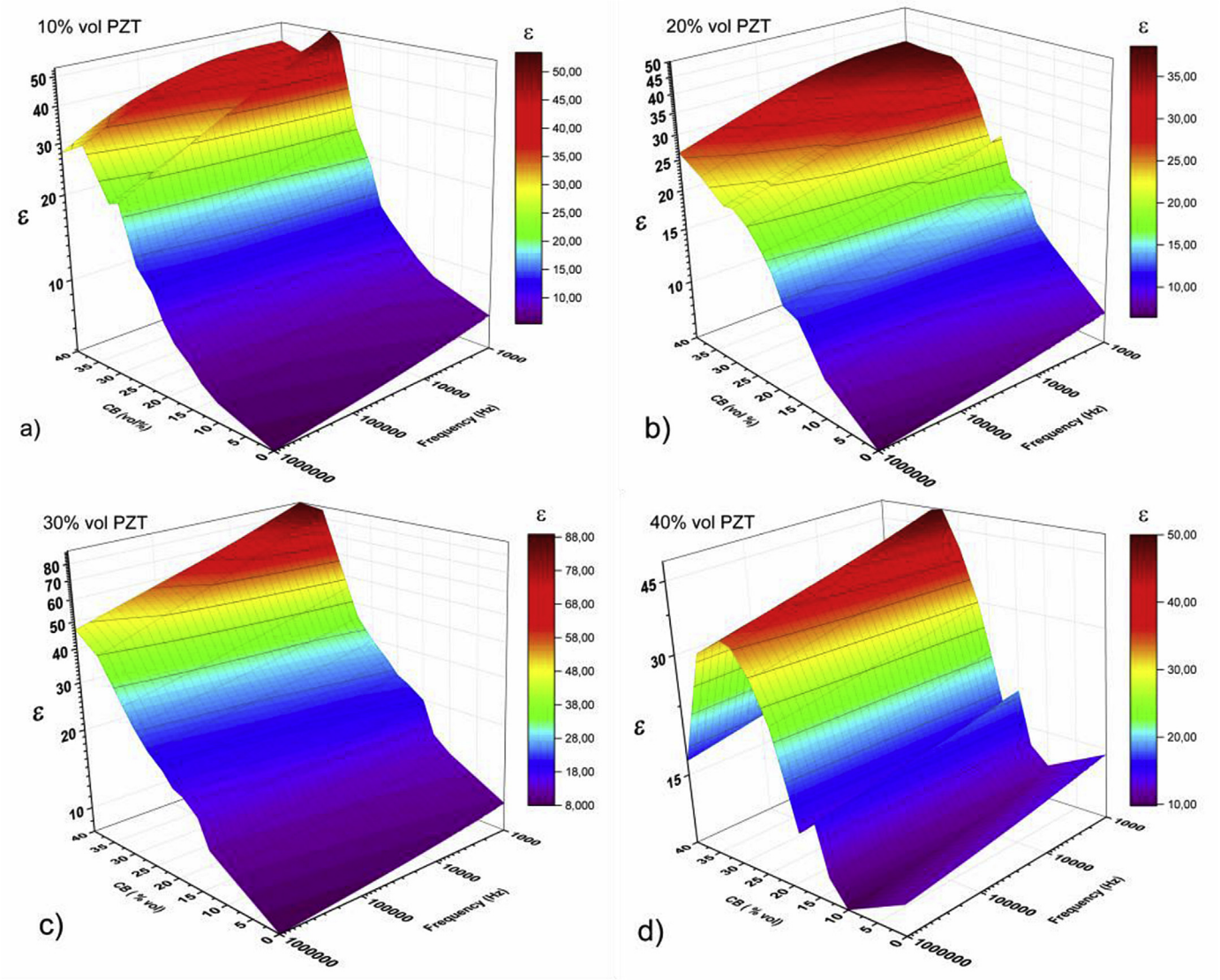

Fig. 6. Dielectric constant frequency dependence of the PU_PZT_CB composites as a function of PZT and CB vol%.

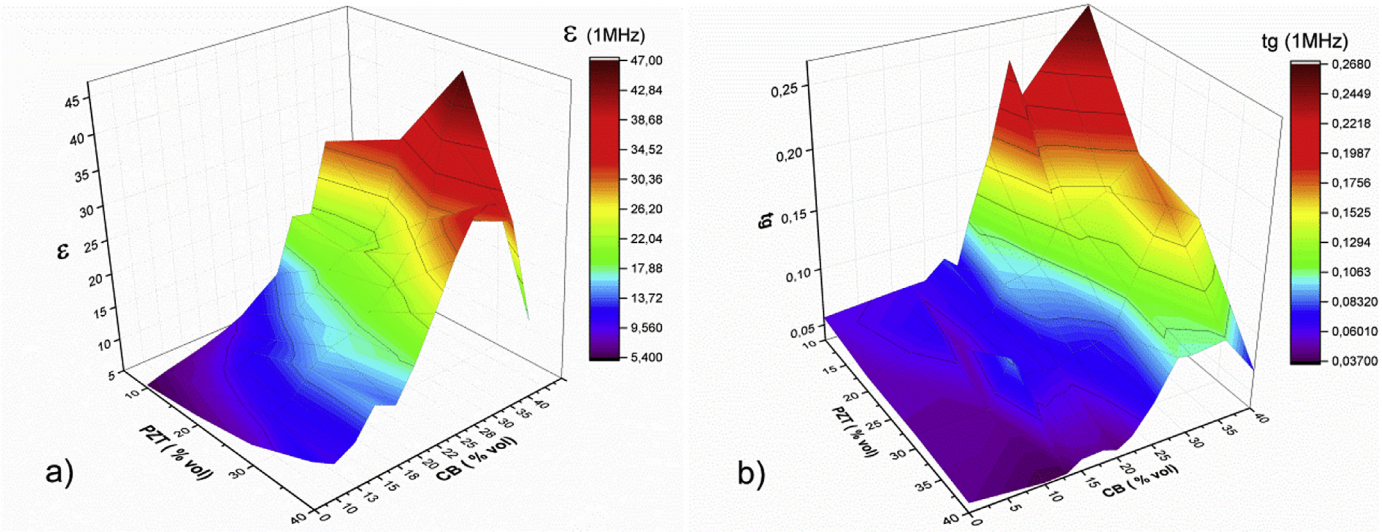

Fig. 7. (a) Dielectric constant and (b) loss tangent of the PU_PZT_CB composites at 1 MHz as a function of the PZT and CB vol%.

exponents; this was attributed to the tunneling effect. The dielectric constant three-phase composites increased gradually as functions of CB, in accordance with the percolation profile.

Acknowledgements

The authors acknowledge the Brazilian agencies, CAPES and CNPq (306753/2012-0) for their financial support.

References

[1] Anthony KELLY (Ed.), Concise Encyclopedia of Composites Materials: Revised Edition, Pergamon, Cambridge, 1994.
[2] S. Nayak, B. Sahoo, T.K. Chakiac, D. Khastgir, Development of polyurethane-titania nanocomposites as dielectric and piezoelectric material, RSC Adv. 8 (2013). http://dx.doi.org/10.1039/C2RA22929C.
[3] M.Z. Dang, J.K. Yuan, J.W. Zha, T. Zhou, S.T. Li, G.H. Hu, Fundamentals, processes and applications of high-permittivity polymer-matrix composites, Prog. Mater Sci. 57 (2012). http://dx.doi.org/10.1016/j.pmatsci.2011.08.001.
[4] S. George, M.T. Sebastian, Three-phase polymer-ceramic-metal composite for embedded capacitor applications, Compos. Sci. Technol. 69 (2009). http://dx.doi.org/10.1016/j.compscitech.2009.03.0031298-1302.
[5] G. Wang, Enhanced Dielectric Properties of Three-phase-percolative composites based on thermoplastic-ceramic matrix (BaTiO3+PVDF) and ZnO radial nanostructures, Acs Appl. Mater Inter. 2 (2010). http://dx.doi.org/10.1021/am100296u.
[6] A.M. Ismail, K.R. Mahmoud, M.H. Abd-El Salam, Electrical conductivity and positron annihilation characteristics of ternary silicone rubber/carbon black/TiB2 nanocomposites, Polym. Test. 48 (2015). http://dx.doi.org/10.1016/j.polymertesting.2015.09.006.
[7] Y. Shen, Y. Guan, Y. Hu, Y. Lei, Y. Song, Y. Lin, C.W. Nan, Dielectric behavior of graphene/BaTiO3/polyvinylidene fluoride nanocomposite under high electric field, Appl. Phys. Lett. 103 (2013). http://dx.doi.org/10.1063/1.4818763.
[8] I.A. Tchmutin, A.T. Ponomarenko, V.G. Shevchenko, N.G. Ryvkina, C. Klason, D.H. McQueen, Electrical transport in 0-3 epoxy resin–barium titanate–carbon black polymer composites, J. Polym. Sci. Part B Polym. Phys. 36 (1998). http://dx.doi.org/10.1002/(SICI)1099-0488(199808)36, 11<1847::AID-POLB6>3.0.CO;2-N.
[9] J.M. Park, H.Y. Lee, J.J. Kim, E.T. Park, Y.K. Chung, Dielectric properties of Ni-coated BaTiO3-PMMA composites, IEEE Trans. Ultrason. Ferroelect., Freq. Control. 55 (2008). http://dx.doi.org/10.1109/TUFFC.2008.752.
[10] X. Dou, X. Liu, Y. Zhang, H. Feng, J.F. Chen, S. Du, Improved dielectric strength of barium titanate-polyvinylidene fluoride nanocomposite, Appl. Phys. Lett. 95 (2009). http://dx.doi.org/10.1063/1.3242004.
[11] S. Tian, X. Wang, Fabrication and performances of epoxy/multi-walled carbon nanotubes/piezoelectric ceramic composites as rigid piezo-damping materials, J. Mat. Sci. 43 (2008). http://dx.doi.org/10.1007/s10853-008-2734-7.
[12] M. Ma, X. Wang, Preparation, microstructure and properties of epoxy-based composites containing carbon nanotubes and PMN-PZT piezoceramics as rigid piezo-damping materials, Mat. Chem. Phys. 116 (2009). http://dx.doi.org/10.1016/j.matchemphys.2009.03.009.
[13] H.W. Choi, Y.W. Heo, J.H. Lee, J.J. Kim, H.Y. Lee, E.T. Park, Y.K. Chung, Effects of BaTiO3 on dielectric behavior of BaTiO3-Ni-polymethyl methacrylate composites, Appl. Phys. Lett. 89 (2006). http://dx.doi.org/10.1063/1.2354425.
[14] S.H. Yao, Z.M. Dang, M.J. Jiang, J. Bai, BaTiO3-carbon nanotube/polyvinylidene fluoride three-phase composites with high dielectric constant and low dielectric loss, Appl. Phys. Lett. 93 (2008). http://dx.doi.org/10.1063/1.3013833.
[15] Z.Y. Xiong, B.Y. Zhang, L. Wang, J. Yu, Z.X. Guo, Modeling the electrical percolation of mixed carbon fillers in polymer blends, Carbon 70 (2014). http://dx.doi.org/10.1016/j.carbon.2014.01.001.
[16] U. Szeluga, B. Kumanek, B. Trzebicka, Synergy in hybrid polymer/nanocarbon composites. A review, Compos. Part A 73 (2015). http://dx.doi.org/10.1016/j.compositesa.2015.02.021.
[17] L. Valentini, S.B. Bon, M.A. Lopez-Manchado, R. Verdejo, L. Pappalardo, A. Bolognini, A. Alvino, S. Borsini, A. Berardo, N.M. Pugno, Synergistic effect of graphene nanoplatelets and carbon black in multifunctional EPDM nanocomposites, Compos. Sci. Technol. 128 (2016). http://dx.doi.org/10.1016/j.compscitech.2016.03.024.
[18] P. Junkong, P. Kueseng, S. Wirasate, C. Huynh, N. Rattanasom, Cut growth and abrasion behaviour, and morphology of natural rubber filled with MWCNT and MWCNT/carbon black, Polym. Test. 41 (2015).
[19] S. Xu, W. Yu, X. Yao, Q. Zhang, Q. Fu, Nanocellulose-assisted dispersion of graphene to fabricate poly(vinyl alcohol)/graphene nanocomposite for humidity sensing, Compos. Sci. Technol. 131 (2016). http://dx.doi.org/10.1016/j.compscitech.2016.05.014.
[20] R. Xu, M. Chen, F. Zhang, X. Huang, X. Luo, C. Lei, S. Lu, X. Zhang, High thermal conductivity and low electrical conductivity tailored in carbon nanotube (carbon black)/polypropylene (alumina) composites, Compos. Sci. Technol. 133 (2016). http://dx.doi.org/10.1016/j.compscitech.2016.07.031.
[21] K. Shehzad, A.A. Hakro, Y. Zeng, S.H. Yao, Y.X. Hong, M. Mumtaz, K. Nadeem, N.S. Khisro, Z.M. Dang, Two percolation thresholds and remarkably high dielectric permittivity in pristine carbon nanotube/elastomer composites, Appl. Nanosci. 5 (2015). http://dx.doi.org/10.1007/s13204-015-0403-0.
[22] X. Wu, C. Lu, X. Zhang, Z. Zhou, Conductive natural rubber/carbon black nanocomposites via cellulose nanowhisker templated assembly: tailored hierarchical structure leading to synergistic property enhancements, J. Mat. Chem. A 3 (2015). http://dx.doi.org/10.1039/C5TA02601F.
[23] E. Enríquez, J. Frutos, J.F. Fernández, M.A. Rubia, Conductive coatings with low carbon-black content by adding carbon nanofibers, Compos. Sci. Technol. 93 (2014). http://dx.doi.org/10.1016/j.compscitech.2013.12.021.
[24] H. Yang, J. Gong, X. Wen, J. Xue, Q. Chen, Z. Jiang, N. Tian, T. Tang, Effect of carbon black on improving thermal stability, flame retardancy and electrical conductivity of polypropylene/carbon fiber composites, Compos. Sci. Technol. 113 (2015). http://dx.doi.org/10.1016/j.compscitech.2015.03.013.
[25] X. Wu, C. Lu, Y. Han, Z. Zhou, G. Yuan, X. Zhang, Cellulose nanowhisker modulated 3D hierarchical conductive structure of carbon black/natural rubber nanocomposites for liquid and strain sensing application, Compos. Sci. Technol. 124 (2016). http://dx.doi.org/10.1016/j.compscitech.2016.01.012.
[26] Z.M. Dang, K. Shehzad, J.W. Zha, A. Mujahid, T. Hussain, J. Nie, C.Y. Shie, Complementary percolation characteristics of carbon fillers based electrically percolative thermoplastic elastomer composites, Compos. Sci. Technol. 72 (2011). http://dx.doi.org/10.1016/j.compscitech.2011.08.020.
[27] R. Schueler, J. Petermann, K. Schulte, H.P. Wentzel, Agglomeration and electrical percolation behavior of carbon black dispersed in epoxy resin, J. Appl. Polym. Sci. 63 (1998). http://dx.doi.org/0.1002/(SICI)1097-4628(19970328)63, 13<1741::AID-APP5>3.0.CO;2-G.
[28] J.R. Harbour, M.J. Walzak, R.P. Veregin, Determination of the origin of the narrow ESR signal in carbon black filled polymers, J. Colloid Interface Sci. 138 (1990). http://dx.doi.org/10.1016/0021-9797(90)90221-9.
[29] L. Flandin, T. Prasse, R. Schueler, K. Schulte, W. Bauhofer, J.-Y. Cavaille, Anomalous percolation transition in carbon-black-epoxy composite materials, Phys. Rev. B Condens. Matter. 59 (1999). https://doi.org/10.1103/PhysRevB.59.14349.
[30] A. Saralegi, M.L. Gonzalez, A. Valea, A. Eceiza, M.A. Corcuera, The role of cellulose nanocrystals in the improvement of the shape-memory properties of castor oil-based segmented thermoplastic polyurethanes, Compos. Sci. Technol. 92 (2014). http://dx.doi.org/10.1016/j.compscitech.2013.12.001.
[31] E. Segal, R. Tchoudakov, M. Narkis, A. Siegmann, Thermoplastic polyurethane - carbon black compounds: structure, electrical conductivity and sensing of liquids, Polym. Eng. Sci. 42 (2002). http://dx.doi.org/10.1002/pen.11129.
[32] M.J. Silva, D.H.F. Kanda, H.N. Nagashima, Mechanism of charge transport in castor oil-based polyurethane/carbon black composite (PU/CB), J. Non-Cryst. Solids. 358 (2012). http://dx.doi.org/10.1016/j.jnoncrysol.2011.09.032.
[33] H.R. Hafiz, Aspects on the percolation and conduction behavior in polypyrrole-poly (vinil chloride) composite, Polym. Bull. 37 (1996). http://dx.doi.org/10.1007/BF00296611.
[34] D.H. McQueen, K.M. Jäger, M. Paligová, Multiple threshold percolation in polymer/filler composites, J. Phys. D. Appl. Phys. 37 (2004). http://dx.doi.org/10.1088/0022-3727/37/15/018.
[35] A.O. Sanches, L.H.S. Ricco, L.F. Malmonge, M.J. Silva, W.K. Sakamoto, J.A. Malmonge, Influence of cellulose nanofibrils on soft and hard segments of polyurethane/cellulose nanocomposites and effect of humidity on their mechanical properties, Polym. Test. 40 (2014). http://dx.doi.org/10.1016/j.polymertesting.2014.08.013.
[36] A. Patsidis, G.C. Psarras, Dielectric behavior and functionality of polymer matrix – ceramic BaTiO3 composites, Express Polym. Lett. 10 (2008). http://dx.doi.org/10.3144/expresspolymlett.2008.85.
[37] Y. Li, X. Huang, Z. Hu, P. Jiang, S. Li, T. Tanaka, Large dielectric constant and high thermal conductivity in poly(vinylidene fluoride)/barium titanate/silicon carbide three-phase nanocomposites, ACS Appl. Mat. Interfaces 3 (2011). http://dx.doi.org/10.1021/am2010459.